# Theoretical consideration of the rheological properties of aggregated suspensions

Cite as: Phys. Fluids **34**, 093309 (2022); https://doi.org/10.1063/5.0103829
Submitted: 17 June 2022 • Accepted: 16 August 2022 • Accepted Manuscript Online: 17 August 2022 • Published Online: 09 September 2022

**Yutaro Tanii** (谷井勇太郎), **Namiko Kamata** (鎌田奈実子), **Hiroki Saito** (斉藤弘樹), **et al.**

Physics of Fluids ARTICLE scitation.org/journal/phf

# Theoretical consideration of the rheological properties of aggregated suspensions

Cite as: Phys. Fluids **34**, 093309 (2022); doi: 10.1063/5.0103829
Submitted: 17 June 2022 · Accepted: 16 August 2022 ·
Published Online: 9 September 2022



Yutaro Tanii (谷井勇太郎),[1] Namiko Kamata (鎌田奈実子),[1] Hiroki Saito (斉藤弘樹),[1] Shusaku Harada (原田周作),[1,a)] and Manabu Sawada (澤田 学)[2]

## AFFILIATIONS

[1]Division of Sustainable Resources Engineering, Faculty of Engineering, Hokkaido University, N13W8, Sapporo, Hokkaido 060-8628, Japan
[2]Murata Manufacturing Co., Ltd., 1-10-1, Higashikotari, Nagaokakyo, Kyoto 617-8555, Japan

[a)]**Author to whom correspondence should be addressed:** harada@eng.hokudai.ac.jp. **Tel./Fax:** +81-11-706-6310

## ABSTRACT

The rheological properties of particulate dispersions containing aggregate structures were theoretically investigated in this study. Under the assumption of Stokes flow, the viscosity of fluids with fine particles was derived by a theoretical method based on the multipole expansion in reciprocal space. In this method, many-body hydrodynamic interactions were considered as the multipole-expanded moment of the force density at the surface of the particles. It is possible to calculate the viscosity of particulate suspensions by considering higher-order moments. The viscosity of monodisperse particulate suspensions was calculated under various conditions. To verify the accuracy of the calculation, the viscosity of uniformly distributed particulate suspensions was calculated, and the results were compared with the experimental results of previous studies. The calculated viscosities were in good agreement with the experimental results for a wide range of particle volumetric concentrations. The viscosity of aggregated suspensions was also calculated to examine the mechanism of viscosity change. The viscosity was systematically calculated with changing the aggregate size and particle concentration. The results indicate that the hydrodynamic effect is not significant on the viscosity change by aggregation, which is contrary to the assumption of previous viscosity models. The calculation results suggest that the increase in the viscosity of aggregated suspensions is instead caused by the direct influence of inter-particle forces.



## INTRODUCTION

The rheological properties of particulate dispersions are important in a wide variety of engineering fields. Understanding these properties is essential to, for example, manufacturing processes in ceramic engineering,[1] the transport of slurries in resources engineering,[2] and the coating of electrode paste in electronic device engineering.[3] It is also important for understanding various natural phenomena, such as lava flows and mudflows in geophysics and geomorphology. Therefore, numerous studies have been conducted beyond the realm of academia.

The mechanism of viscosity change of fluids with fine particles has been explained from the aspect of hydrodynamics. In dilute systems, where hydrodynamic interactions between particles are negligible, it is known that the viscosity increase is caused by stresslets produced by individual particles.[4] In such systems, the viscosity change is expressed as a linear function of particle concentration. In contrast, in systems with large particle concentrations, the hydrodynamic interactions between particles cannot be neglected, and the viscosity becomes a function of higher-order terms of the concentration.[5]

The viscosity of actual particulate suspensions is influenced by various factors in addition to the fluid effect described above. According to Bossis *et al.*,[6] the viscosity can be represented additively by each contribution, as expressed by the following equation:

$$\eta_r = \eta_r^B + \eta_r^I + \eta_r^H, \tag{1}$$

where $\eta_r$ is the ratio of the viscosity of the suspension to that of carrier fluid, $\eta_r^B$ is the contribution of Brownian motion to the viscosity, $\eta_r^I$ is the contribution of particle–particle interactions, and $\eta_r^H$ is the contribution of hydrodynamic interactions. For each of these contributions, there is a complex relationship between the particle concentration, particle size, shear rate, and particle structure. To evaluate the viscosity of particle dispersions precisely, it is important to examine these contributions.

As described in Eq. (1), the rheological properties of particulate suspensions are determined by the balance of forces acting on the particles, namely, the Brownian force $F^B$, inter-particle force $F^I$, and fluid force $F^H$ as well as the particle structures resulting from the balance of

these forces. The significance of each force is expressed by the following dimensionless numbers:

$$Pe = \frac{F^H}{F^B} = \frac{\eta_0 d^3 \dot{\epsilon}_0}{kT}, \tag{2}$$

$$Fa = \frac{F^H}{F^I} = \frac{\eta_0 d^3 \dot{\epsilon}_0}{A}, \tag{3}$$

where $\eta_0$ is the viscosity of the carrier fluid, $d$ is the particle diameter, $\dot{\epsilon}_0$ is the shear rate of carrier flow, $k$ is the Boltzmann constant, $T$ is the absolute temperature, and $A$ is a constant with units of J representing the magnitude of the inter-particle force, such as the Hamaker constant.[7] The Péclet number $Pe$ is the ratio of the contribution of the hydrodynamic force to that of Brownian force. In addition, the Fragmentation number $Fa$ is the ratio of the contribution of the hydrodynamic force to that of the inter-particle force. These two dimensionless numbers determine the significance of each term in Eq. (1).

In actual particulate suspensions, the particles often form aggregate structures due to inter-particle forces. The effect of aggregation on the viscosity has been investigated in previous studies and has been modeled as functions of the particle concentration or aggregate structures.[8–10] In these studies, the fundamental concept of the viscosity model incorporating the effect of aggregates is that the interstitial fluid in aggregates becomes immobile, and the resulting change in the apparent volumetric concentration increases the viscosity. Thus, these viscosity models are based on changes in the hydrodynamic contribution $\eta_r^H$, which is described by the third term in Eq. (1).

However, the mechanism of viscosity change according to the above models, in which the viscosity in aggregated suspensions increases as a result of an increased apparent particle concentration due to immobile fluid in aggregates, has not been clearly verified. As demonstrated in Eq. (1), there are two possible mechanisms of the effect of particle aggregation on viscosity. The first mechanism is based on the hydrodynamic effect described by the third term in Eq. (1), while the second is based on the inter-particle forces described in the second term in Eq. (1). As mentioned above, existing viscosity models in aggregated suspensions are based on the first mechanism. However, according to the second mechanism, the viscosity increases as a result of pairwise inter-particle forces behaving as the source of stress (stresslets). The first mechanism certainly exists; however, whether it produces the excessive viscosity increase associated with particle aggregation remains unclear.

In this study, theoretical analysis of Stokes flow was performed to investigate the mechanism of viscosity change of particulate suspensions with aggregate structures. The hydrodynamic contribution of aggregation to the viscosity change was investigated under large $Pe$ conditions. A theoretical method considering the hydrodynamic interactions between particles was used to calculate the suspension viscosity precisely. The results of the theoretical analysis were validated by a comparison of the viscosity of uniformly distributed particulate suspensions obtained from previous studies as well as various hydrodynamic transport coefficients. Then, assuming aggregate structures of particles without inter-particle forces, the stresslets of particles constituting to the aggregate were calculated. The bulk viscosity of suspensions containing aggregates was calculated from the stresslets, and the influence of the interstitial fluid of loose and dense aggregates, which has been explained by previous viscosity models, was examined.

## THEORETICAL METHOD

### Basic theory

In this study, flow with fine particles is theoretically analyzed based on the formulation of Stokes flow in reciprocal space derived by Ladd.[11–13] Monodisperse particles suspended in a viscous flow at the low Reynolds number limit $Re\ (= \rho d^2 \dot{\epsilon}_0/\eta_0) \to 0$ are considered. Assuming incompressible flow through an infinite particle system consisting of a periodic array of unit cells of volume $V$ containing $N$ particles, the velocity of the surrounding fluid $\boldsymbol{v}(\boldsymbol{r}, t)$ ($\boldsymbol{r}$: position vector, $t$: time) is described by the unsteady Stokes equation and the continuity equation as follows:

$$\rho \frac{\partial}{\partial t} \boldsymbol{v}(\boldsymbol{r}, t) = -\nabla \cdot \boldsymbol{P}(\boldsymbol{r}, t) + \boldsymbol{F}_{\mathrm{ind}}(\boldsymbol{r}, t) \quad |\boldsymbol{r} - \boldsymbol{R}_i(t)| > a, \tag{4}$$

$$\nabla \cdot \boldsymbol{v}(\boldsymbol{r}, t) = 0, \tag{5}$$

where $\rho$ is the fluid density, $\eta_0$ is the viscosity, $a$ is the particle radius, and $\boldsymbol{R}_i(t)$ is the position vector of particle $i$. $\boldsymbol{P}(\boldsymbol{r}, t)$ is the fluid stress tensor and $\boldsymbol{F}_{\mathrm{ind}}(\boldsymbol{r}, t)$ is the induced force per unit volume, i.e., the force density vector exerted on the fluid by particles at their surfaces.[14] The fluid velocity on the surface of particle $i$ is given by

$$\boldsymbol{v}(\boldsymbol{r}, t) = \boldsymbol{U}_i(t) + \boldsymbol{\Omega}_i(t) \times (\boldsymbol{r} - \boldsymbol{R}_i(t)) \quad \text{for } |\boldsymbol{r} - \boldsymbol{R}_i(t)| = a, \tag{6}$$

where $\boldsymbol{U}_i(t)$ and $\boldsymbol{\Omega}_i(t)$ are the translational and angular velocities of particle $i$, respectively. The Fourier transform of Eq. (4) with respect to time $t$ can be written as a function of frequency $\omega$,

$$(-i\omega\rho - \eta_0 \nabla^2) \boldsymbol{v}(\boldsymbol{r}, \omega) = -\nabla p(\boldsymbol{r}, \omega) + \boldsymbol{F}_{\mathrm{ind}}(\boldsymbol{r}, \omega). \tag{7}$$

Taking the divergence of both sides of Eq. (7) and applying the incompressible condition in Eq. (5), the following equation is obtained:

$$\nabla^2 p(\boldsymbol{r}, \omega) = \nabla \cdot \boldsymbol{F}_{\mathrm{ind}}(\boldsymbol{r}, \omega). \tag{8}$$

Two partial differential equations described by Eqs. (7) and (8) can be solved with the Green's functions $G$. Introducing $G(\boldsymbol{r}, \omega) = (4\pi\eta_0 r)^{-1} \exp\left(-\sqrt{-i\omega\rho/\eta_0}\, r\right)$ for Eq. (7) and $G(\boldsymbol{r}, \omega) = (4\pi\eta_0 r)^{-1}$ for Eq. (8), the fluid velocity is obtained as follows:[11]

$$\boldsymbol{v}(\boldsymbol{r}, \omega) = \frac{1}{V} \sum_{\boldsymbol{k} \neq 0} \frac{e^{i\boldsymbol{k}\cdot\boldsymbol{r}}}{-i\omega\rho + \eta_0 k^2} (\boldsymbol{I} - \hat{\boldsymbol{k}}\hat{\boldsymbol{k}}) \cdot \boldsymbol{F}_{\mathrm{ind}}(\boldsymbol{k}, \omega), \tag{9}$$

where $\boldsymbol{I}$ represents the second-rank unit tensor, and $\hat{\boldsymbol{k}} = \boldsymbol{k}/k$ denotes the unit vector in the reciprocal space. The velocity field at steady state is obtained by setting $\omega = 0$ as

$$\boldsymbol{v}(\boldsymbol{r}) = \frac{1}{V} \sum_{\boldsymbol{k} \neq 0} \frac{e^{i\boldsymbol{k}\cdot\boldsymbol{r}}}{\eta_0 k^2} (\boldsymbol{I} - \hat{\boldsymbol{k}}\hat{\boldsymbol{k}}) \cdot \boldsymbol{F}_{\mathrm{ind}}(\boldsymbol{k}), \tag{10}$$

where $\boldsymbol{F}_{\mathrm{ind}}(\boldsymbol{k})$ is the induced force in reciprocal space as follows:

$$\boldsymbol{F}_{\mathrm{ind}}(\boldsymbol{k}) = \int_V e^{-i\boldsymbol{k}\cdot\boldsymbol{r}} \boldsymbol{F}_{\mathrm{ind}}(\boldsymbol{r})\, d\boldsymbol{r}. \tag{11}$$

In Eq. (10), the term $\boldsymbol{k} = 0$ is excluded from the summation with respect to the vector $\boldsymbol{k}$, which is based on the assumption that the net force [$\boldsymbol{F}_{\mathrm{ind}}(\boldsymbol{k} = 0)$ in reciprocal space] is balanced with the ambient pressure gradient in the fluid.[15]

The induced force in real space is the sum of the force density vector $\boldsymbol{f}_j$ acting on the fluid at the surface of particle $j$ as follows:[14]

$$\boldsymbol{F}_{\mathrm{ind}}(\boldsymbol{r}) = \sum_{i=j}^{N} a^{-2}\boldsymbol{f}_j(\hat{\boldsymbol{n}}_j)\delta(|\boldsymbol{r}-\boldsymbol{R}_j|-a), \tag{12}$$

where $\hat{\boldsymbol{n}}_j$ is the unit vector from the center of particle $j$ to its surface. Substituting Eq. (12) into Eq. (11) yields

$$\boldsymbol{F}_{\mathrm{ind}}(\boldsymbol{k}) = \sum_{j=1}^{N} e^{-i\boldsymbol{k}\cdot\boldsymbol{R}_j}\int_{S_j} e^{-i\boldsymbol{k}\cdot\hat{\boldsymbol{n}}_j}\boldsymbol{f}_j(\hat{\boldsymbol{n}}_j)\,d\hat{\boldsymbol{n}}_j, \tag{13}$$

where $S_j$ denotes the surface of particle $j$. The plane wave $e^{i\boldsymbol{k}\cdot\boldsymbol{r}}$ can be expanded by irreducible tensors $\overline{\hat{\boldsymbol{k}}^p}$ and $\overline{\hat{\boldsymbol{r}}^p}$, which are symmetric and traceless:[16]

$$e^{i\boldsymbol{k}\cdot\boldsymbol{r}} = \sum_{p=0}^{\infty} i^p\frac{(2p+1)!!}{p!}j_p(kr)\overline{\hat{\boldsymbol{k}}^p}\odot\overline{\hat{\boldsymbol{r}}^p}, \tag{14}$$

where $j_p$ denotes the spherical Bessel function, $k=|\boldsymbol{k}|$, and $r=|\boldsymbol{r}|$. The operator $\odot$ represents the full contraction between two tensors. From Eqs. (13) and (14), the induced force can be written in the form of a multipole expansion in reciprocal space with the force moment,

$$\boldsymbol{F}_{\mathrm{ind}}(\boldsymbol{k}) = \sum_{j=1}^{N} e^{-i\boldsymbol{k}\cdot\boldsymbol{R}_j}\sum_{p=0}^{\infty}(-i)^p(2p+1)!!j_p(ka)\overline{\hat{\boldsymbol{k}}^p}\odot\boldsymbol{\mathcal{F}}_j^{p+1}, \tag{15}$$

where the force moment $\boldsymbol{\mathcal{F}}_i^{p+1}$ is defined as

$$\boldsymbol{\mathcal{F}}_i^{p+1} \equiv (p!)^{-1}\int_{S_i}\overline{\hat{\boldsymbol{n}}_i^p}\boldsymbol{f}_j(\hat{\boldsymbol{n}}_i)\,d\hat{\boldsymbol{n}}_i. \tag{16}$$

The first and second moments of $\boldsymbol{\mathcal{F}}_i$ correspond to the fluid force $\boldsymbol{F}_i$ and the torque $\boldsymbol{T}_i$ acting on particle $i$ by the fluid and stresslet $\boldsymbol{S}_i$, respectively,

$$\boldsymbol{\mathcal{F}}_i^{1} = -\boldsymbol{F}_i; \quad \boldsymbol{\mathcal{F}}_i^{2a} = (2a)^{-1}\boldsymbol{\varepsilon}:\boldsymbol{T}_i; \quad -a\boldsymbol{\mathcal{F}}_i^{2s} = \boldsymbol{S}_i, \tag{17}$$

where $\boldsymbol{\varepsilon}$ is the Levi-Civita tensor. Superscripts $2a$ and $2s$ denote the asymmetric and symmetric parts of the second-rank tensor, respectively. The moment of fluid velocity at particle surface can be defined in a similar manner as

$$\boldsymbol{\mathcal{U}}_i^{p+1} \equiv \frac{(2p+1)!!}{4\pi a^2}\int\overline{\hat{\boldsymbol{n}}_i^p}(\boldsymbol{v}(\boldsymbol{r})-\boldsymbol{v}_0(\boldsymbol{r}))\delta(|\boldsymbol{r}-\boldsymbol{R}_i|-a)\,d\boldsymbol{r}, \tag{18}$$

where $\boldsymbol{v}_0(\boldsymbol{r})$ denotes the ambient flow velocity in the absence of particles, which is composed of the translational velocity $\boldsymbol{u}_0$, the angular velocity $\boldsymbol{\omega}_0$, and the shear rate $\dot{\boldsymbol{\epsilon}}_0^s$ as

$$\boldsymbol{v}_0(\boldsymbol{r}) = \boldsymbol{u}_0 + \boldsymbol{\omega}_0\times\boldsymbol{r} + \dot{\boldsymbol{\epsilon}}_0^s\cdot\boldsymbol{r}. \tag{19}$$

From the boundary condition at the particle surface given by Eq. (6), the velocity moments are related to the translational velocity, the angular velocity of particle $i$, and the shear rate, such that

$$\boldsymbol{\mathcal{U}}_i^{1} = \boldsymbol{U}_i - \boldsymbol{u}_0; \quad \boldsymbol{\mathcal{U}}_i^{2a} = a\boldsymbol{\varepsilon}\cdot(\boldsymbol{\Omega}_i-\boldsymbol{\omega}_0); \quad \boldsymbol{\mathcal{U}}_i^{2s} = -a\dot{\boldsymbol{\epsilon}}_0^s. \tag{20}$$

From Eqs. (10), (15), and (18), the velocity moments $\boldsymbol{\mathcal{U}}_i^{p+1}$ can be related to the force moments $\boldsymbol{\mathcal{F}}_i^{p'+1}$,

$$\boldsymbol{\mathcal{U}}_i^{p+1} = \sum_{j=1}^{N}\sum_{p'=0}^{\infty}\boldsymbol{\mathcal{G}}_{ij}^{p+1,p'+1}\odot\boldsymbol{\mathcal{F}}_j^{p'+1}, \tag{21}$$

where $p$ and $p'$ represent the order of the velocity and force moments, respectively. In this study, $p=p'$. The coefficient tensor $\boldsymbol{\mathcal{G}}_{ij}^{p+1,p'+1}$ is described as follows:

$$\boldsymbol{\mathcal{G}}_{ij}^{p+1,p'+1} = i^{p-p'}(2p+1)!!(2p'+1)!!\sum_{\boldsymbol{k}\neq 0}e^{i\boldsymbol{k}\cdot(\boldsymbol{R}_i-\boldsymbol{R}_j)} \times\frac{j_p(ka)j_{p'}(ka)}{\eta_0 k^2 V}\overline{\hat{\boldsymbol{k}}^p}(\boldsymbol{I}-\hat{\boldsymbol{k}}\hat{\boldsymbol{k}})\overline{\hat{\boldsymbol{k}}^{p'}}. \tag{22}$$

The calculation of Eq. (21) with the higher order moments $p$ and $p'$ corresponds to a more rigorous consideration of hydrodynamic interactions between particles. Therefore, the accuracy of this method depends on the truncation of the number of these moments $p_{\max}(=p'_{\max})$. For systems with large particle concentrations, it is necessary to consider higher order moments because the hydrodynamic interactions are more significant. However, the accuracy of this method also depends on the problem to be solved, as described later.

## Resistance problem

It follows from Eqs. (17), (20), and (21) that the force and torque exerted on particles by the fluid, and the stresslet are related to the translational and angular velocities of particles and the shear rate, respectively,

$$\begin{bmatrix}\boldsymbol{F}_i\\ \boldsymbol{T}_i\\ \boldsymbol{S}_i\end{bmatrix} = -\sum_{j=1}^{N}\begin{bmatrix}\zeta_{ij}^{TT} & \zeta_{ij}^{TR} & a\zeta_{ij}^{T,2s}\\ \zeta_{ij}^{TR} & \zeta_{ij}^{RR} & a\zeta_{ij}^{R,2s}\\ a\zeta_{ij}^{2s,T} & a\zeta_{ij}^{2s,R} & a^2\zeta_{ij}^{2s,2s}\end{bmatrix}\odot\begin{bmatrix}\boldsymbol{U}_j-\boldsymbol{u}_0\\ \boldsymbol{\Omega}_j-\boldsymbol{\omega}_0\\ -\dot{\boldsymbol{\epsilon}}_0^s\end{bmatrix}, \tag{23}$$

where $\boldsymbol{\zeta}$ is the friction coefficient matrix $\boldsymbol{\zeta}=\boldsymbol{\mathcal{G}}^{-1}$ and the superscripts $T$ and $R$ denote the coefficients relating to translational and rotational motion of particles, respectively. Each component of the friction tensor is described as follows:

$$\begin{gathered}\zeta_{ij}^{TT}=\zeta_{ij}^{1,1}; \quad \zeta_{ij}^{TR}=a\zeta_{ij}^{1,2a}:\boldsymbol{\varepsilon}; \quad \zeta_{ij}^{RT}=-a\boldsymbol{\varepsilon}:\zeta_{ij}^{2a,1};\\ \zeta_{ij}^{RR}=-a^2\boldsymbol{\varepsilon}:\zeta_{ij}^{2a,2a}:\boldsymbol{\varepsilon}, \quad \zeta_{ij}^{T,2s}=\zeta_{ij}^{1,2s}; \quad \zeta_{ij}^{R,2s}=-a\boldsymbol{\varepsilon}:\zeta_{ij}^{2a,2s};\\ \zeta_{ij}^{2s,T}=\zeta_{ij}^{2s,1}; \quad \zeta_{ij}^{2s,R}=a\zeta_{ij}^{2s,2a}:\boldsymbol{\varepsilon}.\end{gathered} \tag{24}$$

The accuracy of Eq. (23) depends on the maximum order of the force and velocity moment $p_{\max}$. For checking the accuracy of this method for various $p_{\max}$ values, the preliminary calculation of two-body problem was conducted. When two particles exist in a static fluid, the force $\boldsymbol{F}$ and torque $\boldsymbol{T}$ acting on each particle are related to the translational velocity $\boldsymbol{U}$ and angular velocity $\boldsymbol{\Omega}$ as follows:

$$\begin{bmatrix}\boldsymbol{F}_1\\ \boldsymbol{F}_2\\ \boldsymbol{T}_1\\ \boldsymbol{T}_2\end{bmatrix} = -\begin{bmatrix}\zeta_{11}^{TT} & \zeta_{12}^{TT} & \zeta_{11}^{TR} & \zeta_{12}^{TR}\\ \zeta_{21}^{TT} & \zeta_{22}^{TT} & \zeta_{21}^{TR} & \zeta_{22}^{TR}\\ \zeta_{11}^{RT} & \zeta_{12}^{RT} & \zeta_{11}^{RR} & \zeta_{12}^{RR}\\ \zeta_{21}^{RT} & \zeta_{22}^{RT} & \zeta_{21}^{RR} & \zeta_{22}^{RR}\end{bmatrix}\odot\begin{bmatrix}\boldsymbol{U}_1\\ \boldsymbol{U}_2\\ \boldsymbol{\Omega}_1\\ \boldsymbol{\Omega}_2\end{bmatrix}, \tag{25}$$

where numerical subscripts indicate the particle number. The above expression is known as the resistance problem. In the case of two-body resistance problem, each component tensor $\boldsymbol{\zeta}$ in Eq. (25) can be

expressed by combinations of scalar functions.[17] For example, $\zeta_{11}^{TT}$ is expressed as follows:

$$\zeta_{11}^{TT} = X_{11}^{A}\boldsymbol{ee} + Y_{11}^{A}(\boldsymbol{\delta} - \boldsymbol{ee}), \tag{26}$$

where $\boldsymbol{e}$ denotes the unit vector directed from one to another particles and $\boldsymbol{\delta}$ is the Kronecker delta. $X_{11}^{A}$ and $Y_{11}^{A}$ indicate the scalar resistance functions.[17] The exact solution of the scalar resistance functions of two equal-sized spherical particles was derived by Jeffrey and Onishi.[18] For example, the scalar function $X_{11}^{A}$ is expressed by particle center-to-center distance $r$ as follows:

$$\begin{aligned} X_{11}^{A} &= g_1(1-4r^{-2})^{-1} - g_2\ln(1-4r^{-2}) \\ &\quad - g_3(1-4r^{-2})\ln(1-4r^{-2}) + f_0 - g_1 \\ &\quad + \sum_{m=2(\text{even})}^{\infty}\left(2^{-2m}f_m - g_1 - 2m^{-1}g_2 + 4m^{-1}m_1^{-1}g_3\right)\left(\frac{2}{r}\right)^{m}, \end{aligned} \tag{27}$$

where

$$m_1 = -2\delta_{m2} + (m-2)(1-\delta_{m2})$$

and

$$\begin{gathered} g_1 = 1/4, \quad g_2 = 9/40, \quad g_3 = 3/112, \\ f_0 = 1, \quad f_1 = 3, \quad f_2 = 9, \quad f_3 = 19, \quad f_4 = 93, \\ f_5 = 387, \quad f_6 = 1197, \quad f_7 = 5331, \quad f_8 = 19\,821, \\ f_9 = 76\,115, \quad f_{10} = 320\,173, \quad f_{11} = 1\,178\,451, \end{gathered}$$

respectively.

We solved the above-mentioned two-body problem approximately. We set two particles in a large-sized calculation cell for avoiding the effect of the periodic boundary and calculated the scalar functions stated above. The length of calculation cell is set to be constant as $L = 20a$ ($a$: particle radius), and the inter-particle distance (surface-to-surface distance) $L_{\min}(= r - 2a)$ is changed. Figure 1 indicates the scalar function $X_{11}^{A}$ for the calculation with $p_{\max}$ from 1 to 6.

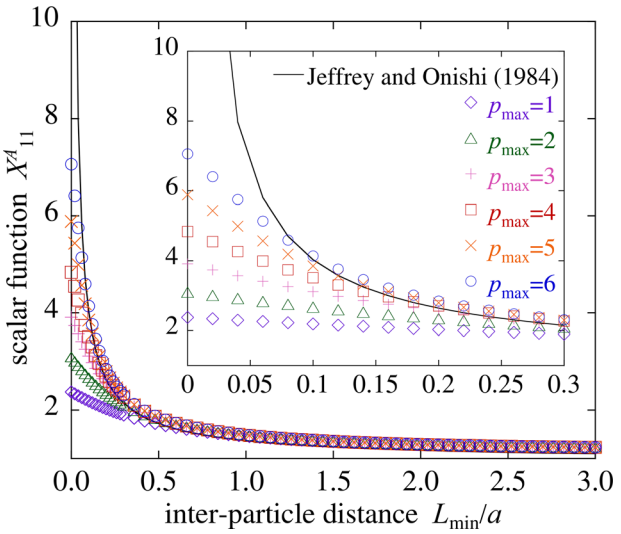


**FIG. 1.** Scalar function $X_{11}^{A}$ of two-body resistance problem as a function of inter-particle distance $L_{\min}/a$ for various $p_{\max}$ values.

The solid line indicates the exact solution given in Eq. (27). If the inter-particle distance is large enough, the obtained scalar function agrees well with the exact one regardless of $p_{\max}$. By contrast, when the inter-particle distance is smaller than $L_{\min} = 0.5$, $X_{11}^{A}$ for small $p_{\max}$ deviates from the exact solution. As shown in Fig. 1, the calculation with $p_{\max} = 6$ keeps accuracy for the inter-particle distance $L_{\min}/a > 0.08$. This value of the inter-particle distance corresponds to dense particle systems. Taking the regular structure of particle layers as examples, it is found from simple geometric calculations that the particle volume fraction $\phi = 0.47$ for simple cubic (SC), $\phi = 0.6$ for body-centered cubic (BCC), and $\phi = 0.66$ for face-centered cubic (FCC) particle layers. Based on the above results, we set $p_{\max} = 6$ in this study because the calculation keeps accuracy at dense particle volume fraction close to the maximum packing.

## Calculation of viscosity

The viscosity of particulate suspension can be calculated from Eq. (23). For incompressible, isotropic, and Newtonian fluids, the viscosity is independent of the shear direction. Focusing only on the $xy$ component, Newton's viscous law states that the shear stress is proportional to the shear rate,

$$\sigma_{xy} = \eta\dot{\epsilon}_{xy}^{s}, \tag{28}$$

where $\eta$ is the viscosity of the suspension, $\sigma_{xy}$ and $\dot{\epsilon}_{xy}^{s}$ are the $xy$ components of the shear stress and shear rate in the presence of particles, respectively. The shear stress of the suspension consists of the contribution from the ambient shear flow and the contribution from the disturbance of the flow by particles, $\sigma_{xy} = \sigma_{\text{fluid},xy} + \sigma_{\text{ind},xy}$. Here, $\sigma_{\text{fluid},xy}$ denotes the shear stress caused by the ambient shear flow,

$$\sigma_{\text{fluid},xy} = \eta_0\dot{\epsilon}_{xy}, \tag{29}$$

where $\eta_0$ is the fluid viscosity. $\sigma_{\text{ind},xy}$ is calculated from the stresslet of each particle,

$$\sigma_{\text{ind},xy} = V^{-1}\sum_{i=1}^{N} S_{i,xy} = \frac{3\phi}{4\pi a^3 N}\sum_{i=1}^{N} S_{i,xy}, \tag{30}$$

where $V$ represents the volume of the unit cell containing $N$ particles and is expressed as $V = \left(N \times \frac{4}{3}\pi a^3\right)/\phi$ using the particle volume fraction $\phi$. Under the condition of low particle inertia, particles move following the ambient flow, signifying that no fluid or torque is exerted on them. Expanding Eq. (23) for $\boldsymbol{S}_i$ and substituting $\boldsymbol{F}_i = 0$ and $\boldsymbol{T}_i = 0$,

$$S_{i,xy} = a^2\sum_{j=1}^{N}\tilde{\zeta}_{ij,xykl}^{2s,2s}\dot{\epsilon}_{0,lk}^{s}, \tag{31}$$

where $\tilde{\zeta}_{ij}^{2s,2s}$ is the modified form of $\zeta_{ij}^{2s,2s}$ incorporating the zero force and zero torque condition,

$$\tilde{\zeta}_{ij}^{2s,2s} = \zeta_{ij}^{2s,2s} - \begin{bmatrix}\zeta_{ij}^{2s,T} & \zeta_{ij}^{2s,R}\end{bmatrix}\cdot\begin{bmatrix}\zeta_{ij}^{TT} & \zeta_{ij}^{TR} \\ \zeta_{ij}^{RT} & \zeta_{ij}^{RR}\end{bmatrix}^{-1}\cdot\begin{bmatrix}\zeta_{ij}^{T,2s} \\ \zeta_{ij}^{R,2s}\end{bmatrix}. \tag{32}$$

If the system is isotropic, $\tilde{\zeta}_{ij}^{2s,2s}$ can be regarded as the fourth-rank isotropic tensor. Therefore, all components excluding $(k,l) = (x,y)$, $(y,x)$ of the inner-product in Eq. (31) are zero. $\tilde{\zeta}_{ij}^{2s,2s}$ and $\dot{\epsilon}_{0}^{s}$ are both symmetric tensors, therefore,

$$S_{i,xy} = \frac{20}{3}\pi\eta_0 a^3 \gamma^{2s,2s}_{i,xyxy}\dot{\epsilon}^s_{0,xy}, \tag{33}$$

where $\gamma^{2s,2s}_{i,xyxy}$ is the normalized form of $\sum_{j=1}^{N}\zeta^{2s,2s}_{ij,xyxy}$ with its low-density limit $\zeta^{2s,2s}_0 = (10/3)\pi\eta_0 a$.[13]

Combining Eqs. (29), (30), and (33), the shear stress is given by

$$\sigma_{xy} = \eta_0\left(1 + \frac{5}{2}\phi\frac{1}{N}\sum_{i=1}^{N}\gamma^{2s,2s}_{i,xyxy}\right)\dot{\epsilon}_{xy}, \tag{34}$$

where the difference between $\dot{\epsilon}^s$ and $\dot{\epsilon}^s_0$ is negligible for periodic boundary conditions. Comparing Eqs. (28) and (34), the relative viscosity is obtained as

$$\eta^H_r = \frac{\eta}{\eta_0} = 1 + \frac{5}{2}\phi\langle\gamma^{2s,2s}_{xyxy}\rangle, \tag{35}$$

where $\langle\cdots\rangle$ denotes the ensemble average over $N$ particles. $\langle\gamma^{2s,2s}_{xyxy}\rangle = 1$ for a dilute suspension, which leads to Einstein's viscosity formula,[4]

$$\eta^H_r|_{\phi\to 0} = 1 + \frac{5}{2}\phi. \tag{36}$$

## Verification of theoretical method

Various hydrodynamic coefficients other than viscosity can be derived from the coefficient tensor $\mathcal{G}^{p+1,p'+1}_{ij}$ in Eq. (22).[13] As mentioned in the Introduction, the main purpose of this study is to examine the viscosity of particulate suspensions containing aggregate structures. Before discussing the main topic, the calculation results of other hydrodynamic coefficients that can be obtained by this method are presented. By comparing the results with those obtained in previous studies, the accuracy of this analysis is verified. It should be noted that the demonstrations presented here are basically identical to those given by Ladd.[13]

First, the permeability of a fixed particle bed is derived. The flow permeating through the particle layer with translational velocity $\boldsymbol{v}(\boldsymbol{r}) = \boldsymbol{u}_0$ is considered. If the system is isotropic, the permeability can be regarded as a scalar quantity $K$ that is independent of the flow direction. In this case, the pressure gradient $\nabla p$ and the mean flow velocity $\boldsymbol{u}_0$ are related by the permeability $K$ using Darcy's law,

$$\nabla p = -\eta_0 K^{-1}\boldsymbol{u}_0. \tag{37}$$

At steady state, the pressure gradient is balanced by the force per unit volume exerted on the fluid by the particles,

$$\nabla p = -V^{-1}\sum_{i=1}^{N}\boldsymbol{F}_i. \tag{38}$$

From Eq. (23), it follows from the force $\boldsymbol{F}_i$ related to the fluid velocity via the friction coefficient matrix $\boldsymbol{\zeta}^{TT}$ that Eq. (38) can be written as

$$\nabla p = -V^{-1}\sum_{i,j=1}^{N}\boldsymbol{\zeta}^{TT}_{ij}\cdot\boldsymbol{u}_0, \tag{39}$$

where the translational and angular velocities of the particles are zero because the particles are immobile. For an isotropic system, $\boldsymbol{\zeta}^{TT}_{ij}$ is the second-rank isotropic tensor, i.e., $\sum_{i,j=1}^{N}\boldsymbol{\zeta}^{TT}_{ij} = \frac{1}{3}\mathrm{tr}(\sum_{i,j=1}^{N}\boldsymbol{\zeta}^{TT}_{ij})\boldsymbol{I}$, therefore,

$$\nabla p = -V^{-1}\frac{1}{3}\mathrm{tr}\left(\sum_{i,j=1}^{N}\boldsymbol{\zeta}^{TT}_{ij}\right)\boldsymbol{u}_0. \tag{40}$$

Combining Eqs. (40) and (37), the permeability $K$ can be expressed in the inverse form:

$$K^{-1} = (\eta_0 V)^{-1}\frac{1}{3}\mathrm{tr}\left(\sum_{i,j=1}^{N}\boldsymbol{\zeta}^{TT}_{ij}\right). \tag{41}$$

Figure 2 illustrates the dimensionless permeability $K^* = K/a^2$ in a randomly distributed particle bed obtained from Eq. (41) with particle volume fraction $\phi$. The solid line indicates the permeability theoretically obtained by Brinkman[19] as follows:

$$K^* = \frac{2}{9\phi}\left(1 + \frac{3}{4}\phi\left[1 - \sqrt{\frac{8}{\phi} - 3}\right]\right). \tag{42}$$

Equation (42) is derived on the assumption of a dilute particle concentration. The dashed line in Fig. 2 indicates the well-known Kozeny–Carman equation derived semi-empirically as

$$K^* = \frac{(1-\phi)^3}{45\phi^2}, \tag{43}$$

where the Kozeny constant is set to 5.[20] Equation (43) is valid for moderate to dense concentrations. Both Eqs. (42) and (43) are decreasing functions with $\phi$, which indicates that the flow is less permeable in particle beds with large concentrations. The plots in Fig. 2 display the

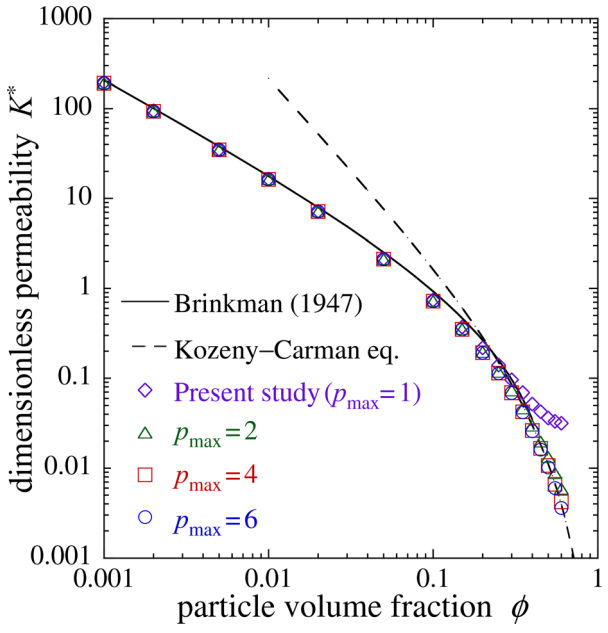


**FIG. 2.** Dimensionless permeability of a fixed particle bed as a function of particle volume fraction.

permeability obtained from this method with changing the maximum order of the force and velocity moments $p_{max}$ from 1 to 6. Focusing on a dilute concentration $\phi < 0.2$, the theoretical results for all $p_{max}$ conditions agree well with the Brinkman equation presented in Eq. (42). However, the results with $p_{max} = 1$ deviate from the Brinkman equation at a moderate concentration of $\phi \sim 0.2$. At dense concentrations, the results with $p_{max}$ from two to six quantitatively agree with the Kozeny–Carman equation given by Eq. (43). This indicates that the above theory can properly calculate the hydrodynamic interactions between particles, and that the calculation with $p_{max} = 2$ is adequate for the calculation of the permeability from dilute to dense concentrations close to the maximum packing of $\phi \sim 0.6$.

Next, the drag force exerted on a particle in a particulate suspension is derived. In Stokes flow, it is known that the drag force in a suspension consisting of spherical particles can be obtained analytically as a function of the particle volume fraction $\phi$. Brinkman[19] theoretically derived the drag force in a dilute suspension. With the help of the considerations of van der Hoef,[21] the normalized drag force acting on each particle $F^* = F/6\pi\mu a u_0$ is described as follows:

$$F^* = (1-\phi)\left(1+\frac{3}{4}\phi\left[1-\sqrt{\frac{8}{\phi}-3}\right]\right)^{-1}. \tag{44}$$

For dilute to dense suspensions, Koch and Sangani[22] proposed the drag force in suspensions as follows:

$$F^* = \begin{cases} \dfrac{(1-\phi)\left(1+\frac{3}{\sqrt{2}}\phi^{1/2}+\frac{135}{64}\phi\ln\phi+16.14\phi\right)}{1+0.681\phi-8.48\phi^2+8.16\phi^3} & (\phi<0.4), \\ 10\dfrac{\phi}{(1-\phi)^2} & (\phi>0.4). \end{cases} \tag{45}$$

Figure 3 shows the relationship between the normalized drag force $F^*$ and the particle volume fraction $\phi$. In this analysis, the drag force is calculated from the force balance of particle and fluid using the permeability in Eq. (41) as follows:

$$F^* = \frac{2(1-\phi)}{9\phi K^*}. \tag{46}$$

The results of the analysis illustrated in Fig. 3 are obtained from calculation with $p_{max} = 6$. The theoretical and numerical results of previous studies are also indicated in the figure. The solid line indicates the theoretical results by Brinkman given by Eq. (44), while the dashed line indicates the results by Koch and Sangani given by Eq. (45). The open symbols denote the numerical results using the Lattice-Boltzmann Method (LBM) by van der Hoef *et al.*[21] and Hill *et al.*[23]

At the low concentration limit, the drag force is close to $F^* = 1$, i.e., the Stokes drag $F = 6\pi\eta_0 a u_0$. As the particle volume fraction increases, the drag force increases gradually. At dilute concentrations, the theoretical and numerical results are in almost perfect agreement with the Brinkman equation, whereas at moderate to dense concentrations, they are almost along with the results by Koch and Sangani.[22] A comparison of the theoretical results obtained in this study with the others, and the present results somewhat overestimate the drag force at dense concentrations, although the results shown here are calculated

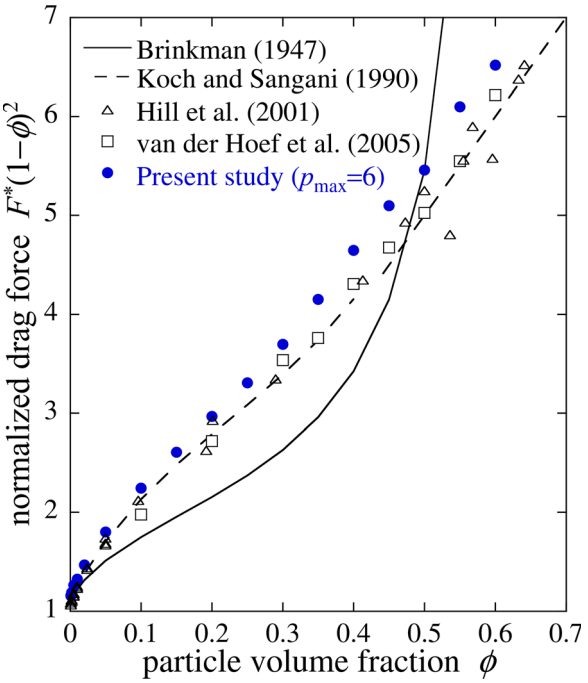


**FIG. 3.** Normalized drag force acting on randomly arranged particles as a function of particle volume fraction.

considering high order moments ($p_{max} = 6$). This indicates that higher order moments must be considered in the calculation of the drag force of a suspension for large concentrations.

The reason for the difference in the precision between the calculations of the permeability and drag force, which are given in Figs. 2 and 3, is that the drag force is calculated from the inverse of the permeability. It is known that there are two approaches for solving the particle motion in Stokes flow, i.e., the resistance problem and mobility problem.[17] In the analysis, the calculation of the permeability and drag force corresponds to the mobility and resistance problems, respectively. In general, the resistance problem at large particle concentrations is more sensitive than the mobility problem. Therefore, a higher order calculation is required for the calculation of the drag force. For solving the resistance problem at large concentrations with high precision, special treatments, such as lubrication correction, are required.[13] The above two demonstrations indicate that the theoretical analysis in this study can successfully represent the hydrodynamic transport coefficients of particulate suspensions, and that the calculation precision greatly depends on the problem to be solved.

## RESULTS AND DISCUSSION

### Viscosity of uniform suspension

The relative viscosity of particulate suspension $\eta_r^H$ was calculated from Eq. (35) for various concentrations and particle arrangements, i.e., the particles are dispersed uniformly, or they make aggregates in fluid. To verify the accuracy of the calculation, the results of the viscosity of the uniform suspension were compared to those obtained in previous experimental studies.

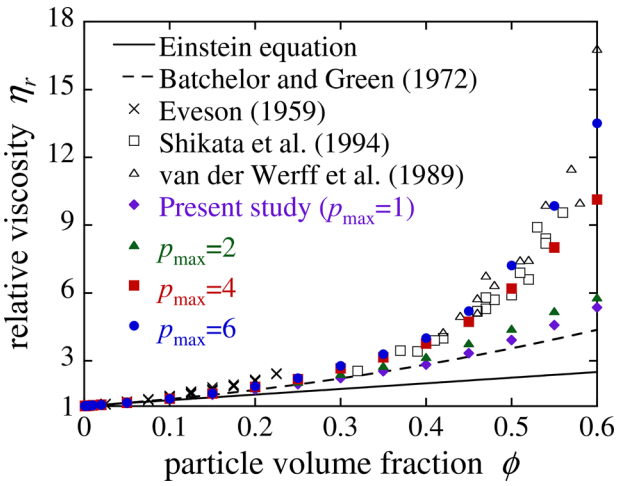


**FIG. 4.** Relative viscosity of uniformly distributed particulate suspensions.

Figure 4 presents the relationship between the relative viscosity and the particle volume fraction for a uniformly dispersed suspension of particles. The closed symbols denote the analytical results, which were obtained from Eq. (35) by varying the maximum order of the moments $p_{max}$. The solid line denotes the Einstein equation given in Eq. (36), which does not take into account the hydrodynamic interactions between particles, and the dashed line denotes the solution for semi-dilute suspension by Batchelor and Green[24] as follows:

$$\eta_r^H = 1 + \frac{5}{2}\phi + 5.2\phi^2. \tag{47}$$

The open symbols represent the results of previous experiments.[25–27] For small particle concentrations, the analytical results of relative viscosity are consistent with the Einstein equation for all orders of calculation and exhibit a linear relationship with the particle volume fraction.

As the particle concentration increases above $\phi = 0.1$, the experimental and analytical results deviate from the Einstein equation and exhibit nonlinear features. This indicates that the influence of hydrodynamic interactions becomes significant, and that the summation of isolated particle stresslets can no longer represent the viscosity at non-dilute concentrations. The analytical results for small $p_{max}$ do not fully capture the nonlinear changes observed in the experiments at large concentrations, while the results for large $p_{max}$ (= 4–6) approximately represent the experimental results at small to large concentrations. This is because the higher-order terms of velocity and force moments become non-negligible as the average inter-particle distance decreases, as is shown in Fig. 1. These results indicate that the present analysis taking into account higher-order moments can approximately reproduce the rheological properties of particulate suspensions for a wide range of concentrations.

## Viscosity of aggregated suspension

When the suspended particles are unevenly but isotropically distributed, i.e., the particles form aggregates, the viscosity of suspensions would change. As described in Eq. (1), the viscosity change of particulate suspensions can be explained by three factors: Brownian motion, inter-particle forces, and hydrodynamic effects. Several studies have been reported that the effect of aggregates on viscosity is due to changes in the apparent particle concentration as the interstitial fluid of the aggregate becomes immobile.[8–10] The viscosity model derived under such assumptions is, for example, can be described as follows:[8]

$$\eta_r^H = \frac{1 - \phi_{\mathrm{eff}}}{\left(1 - \frac{\phi_{\mathrm{eff}}}{\phi^*}\right)^2}, \tag{48}$$

where $\phi_{\mathrm{eff}}$ is the effective volumetric concentration and $\phi^*$ is the concentration of maximum random packing (e.g., $\phi^* = 0.64$). In this model, the volume of immobile fluid is determined by considering the space-filling properties of the aggregate (e.g., fractal dimension) when calculating the effective concentration. This model contains the inter-particle force as a parameter, which determines the morphological properties of the aggregate but does not contribute to the viscosity change directly. Therefore, it should be noted that the contribution of inter-particle force in the previous model is reflected in $\eta_r^H$, not $\eta_r^I$ of Eq. (1).

In order to investigate whether the interstitial fluid in aggregates contributes to the hydrodynamic viscosity change, the viscosity of suspensions with aggregate structures was calculated. The suspended particles were locally concentrated by decreasing the inter-particle distance from a uniform dispersion state. The inter-particle distance was changed from $L_{\mathrm{min}}/a = 4$ to $L_{\mathrm{min}}/a = 0.1$ within the range where the accuracy of this analysis was maintained, as shown in Fig. 1. Figure 5 presents the analytical results of viscosity of locally concentrated suspensions for the particle volume fraction $\phi = 0.01$ and the number of particles $N = 55$. In the analysis, the maximum order of moments $p_{max}$ changes from 1 to 6. As mentioned above, the analysis is based on a multipole expansion in reciprocal space, which corresponds to an infinite periodic array of particle structures. Therefore, the system considered here consists of periodically located aggregates in a fluid. In Fig. 5, the lower horizontal axis represents the minimum distance between particles in the aggregate, while the upper represents

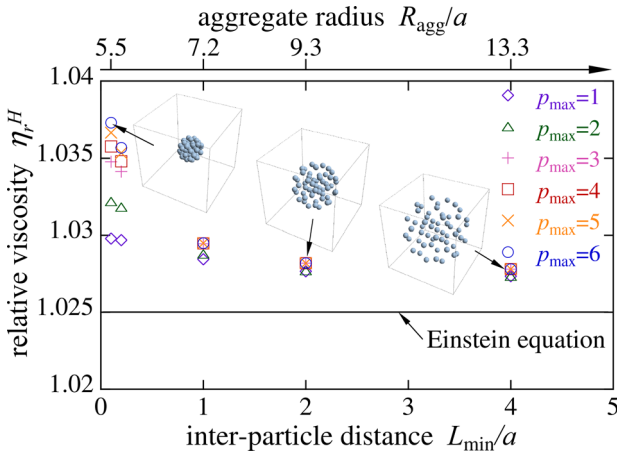


**FIG. 5.** Relationship between the relative viscosity and minimum inter-particle distance in aggregated suspensions.

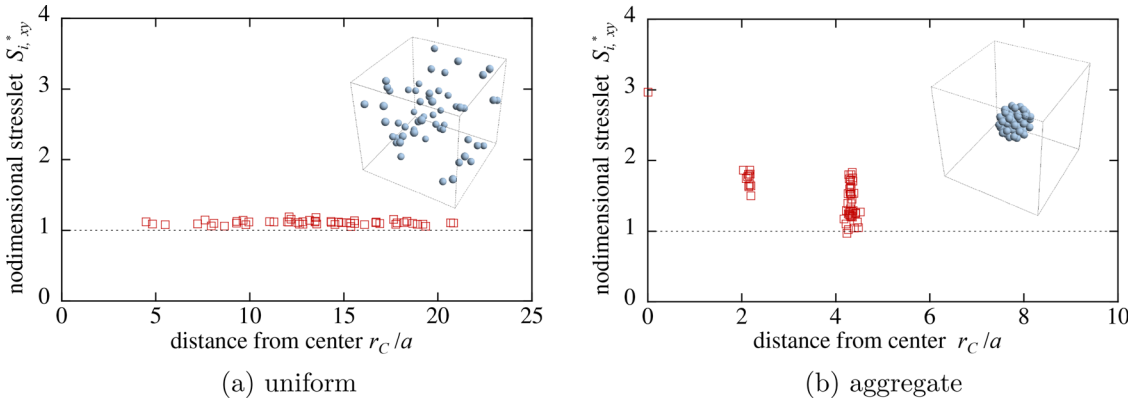


**FIG. 6.** Relationship between the stresslet and distance from the center in (a) uniform and (b) aggregated suspensions for $\phi = 0.01$.

the aggregate radius. Therefore, Fig. 5 illustrates the transition from large and loose aggregates (right) to small and compact aggregates (left). In general, the inter-particle force of the colloidal system, such as van der Waals force, is short-ranged;[7] therefore, the aggregate with $L_{\min}/a = 4$ has somewhat an unrealistic structure. The reason for assuming such loose aggregates is to systematically investigate the effect of interstitial fluid on the viscosity.

When the inter-particle distance is large, i.e., the particles form loose aggregates, the viscosity is asymptotically close to that obtained from the Einstein equation. The viscosity increases as the inter-particle distance decreases, and the particles form compact aggregates. Most compact aggregate is formed at an aggregate radius of $R_{\text{agg}}/a = 5.5$ for $L_{\min}/a = 0.1$; however, the viscosity increases only a few percent. There is almost no dependence of the viscosity on the maximum order $p_{\max}$ at large inter-particle distances, whereas there is a considerable dependence for the most compacted aggregate.

As shown in Fig. 4, the analytical results of the viscosity of uniform suspensions for $p_{\max} = 4$–$6$ are in approximate agreement with the experimental results. As also shown in Fig. 5, the change in viscosity decreases as $p_{\max}$ increases, and there is tiny difference between the results for $p_{\max} = 5$ and 6 in the limit of small inter-particle distance. Based on these results, the results for $p_{\max} = 6$ are presented in the subsequent analysis of aggregated suspensions.

## Stresslet distribution

To more thoroughly investigate the viscosity change due to aggregation, the stresslet induced by individual particles was examined. Figures 6 and 7 show the distribution of the nondimensional stresslet $S^*_{i,xy} = \gamma^{2s,2s}_{i,xyxy}$ of a uniform suspension and a suspension with dense aggregates at the particle volume fractions of $\phi = 0.01$ and $\phi = 0.15$, respectively. The horizontal axis represents the distance to each particle from the center of mass of the particles in the calculation domain $r_C/a$, while the vertical axis represents the stresslet of each particle. The minimum inter-particle distance in dense aggregates is $L_{\min}/a = 0.1$.

As illustrated in Fig. 6(a), in the dilute uniform suspension ($\phi = 0.01$), the nondimensional stresslets of particles are almost uniformly distributed, and their value is approximately one. This is because each particle contributes to the viscosity of the system as an isolated stresslet, similar to the assumption of the Einstein equation. In contrast, in the non-dilute random suspension ($\phi = 0.15$) illustrated in Fig. 7(a), the stresslets exhibit larger and more scattered values. This indicates that the hydrodynamic interactions between particles become significant as the particle concentration increases, and that small variations in the inter-particle distance cause substantial changes in the stresslet of each particle.

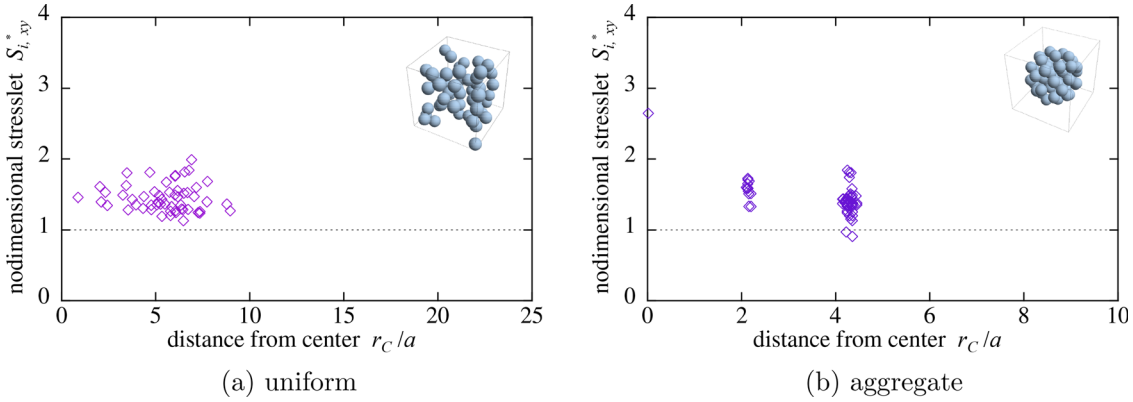


**FIG. 7.** Relationship between the stresslet and distance from the center in (a) uniform and (b) aggregated suspensions for $\phi = 0.15$.

In the locally aggregated suspensions ($\phi = 0.01$) shown in Fig. 6(b), the stresslet of each particle varies greatly depending on the relative position of particles in the aggregate. As shown in the figure, the aggregate considered here has a concentric layered structure. The stresslets of particles outside the aggregate are approximately one or slightly larger than one. The stresslet increases as one approaches the center of aggregate, reaching a maximum value at the central particle. Even at the dilute concentration, the stresslet of each particle increases due to hydrodynamic interactions as the particles become locally dense. In the aggregated suspension for $\phi = 0.15$ in Fig. 7(b), the stresslet of a particle near the center of the aggregate is almost the same as that for $\phi = 0.01$. This is caused by the screening effect of hydrodynamic interactions,[35] i.e., long-range hydrodynamic interactions decay in the aggregate, and the stresslet of the center particle is determined almost entirely by the local particle arrangement. The particles at the outer edges of the aggregate exhibit scattered stresslets; however, there is no significant difference between conditions of $\phi = 0.01$ and $\phi = 0.15$.

In order to gain insight into the screening effect of hydrodynamic interactions inside an aggregate, the relationship between the local concentration and stresslet at each particle location was investigated. The locally averaged concentration $\phi_L$ was obtained by averaging the particle existence function $\rho(x, y, z) = 0$ or 1 using a weight function. In this study, a Gaussian function was used as the weight function,

$$g(x, y, z) = \frac{1}{\sqrt{2\pi}^3 \lambda^3} \exp\left(-\frac{x^2 + y^2 + z^2}{2\lambda^2}\right), \tag{49}$$

where $\lambda$ is a parameter that determines the amount of local averaging and $\lambda = 2.5a$ in this study. Using Eq. (49), the local concentration $\phi_L$ can be obtained as follows:

$$\phi_L(x, y, z) = \int\int\int_{-\infty}^{\infty} g(x - x', y - y', z - z')\rho(x', y', z')dx'dy'dz'. \tag{50}$$

Figure 8 shows the stresslet distribution of aggregated suspensions for particle concentrations $\phi = 0.01$ and $\phi = 0.15$. The horizontal axis denotes the local concentration at each particle location. In aggregated suspensions, the local concentration $\phi_L$ depends on the relative position in the aggregate. The local concentration increases from the outside to the inside of the aggregate. For more quantitative discussion, the results in Fig. 8 are compared with the stresslet of uniform suspensions. As shown in Fig. 4, the viscosity of uniform suspension increases with the concentration. Many theoretical, semi-empirical viscosity models of uniform suspension have been proposed as a function of the particle volume fraction $\phi$.[28–33] For example, Mendoza *et al.*[34] proposed the following model as a polynomial of $\phi$:

$$\eta_r^H = 1 + 2.5\phi + 4.5\phi^2 + 7\phi^3 + 10\phi^4 + 13.5\phi^5 + 17.5\phi^6 + 22\phi^7 + O(\phi^8). \tag{51}$$

The solid line in Fig. 8 indicates the theoretical curve of a non-dimensional stresslet of uniform suspensions, which is calculated from Eqs. (33), (35), and (51),

$$S^*_{i,xy} = 1 + 1.8\phi + 2.8\phi^2 + 4\phi^3 + 5.4\phi^4 + 7\phi^5 + 8.8\phi^6 + O(\phi^7). \tag{52}$$

As can be seen in Fig. 8, the stresslet of each particle approximately corresponds to the theoretical stresslet at each local concentration. This indicates that the inner particles are shielded by the surrounding particles, resulting in a locally dense structure. In consequence, the stresslets of particles near the center of the aggregate are not influenced by other aggregates and are determined only by their relative position (i.e., local concentration) in the aggregate. For the outer particles, the stresslets are slightly smaller than the theoretical values due to an anisotropic particle arrangement, i.e., one side is dense and the other side is sparse. Note that if the aggregate is a loose structure, the shielding effect will be significantly reduced.

## Hydrodynamic effect on viscosity of aggregated suspension

Finally, the effective viscosity of the entire system is demonstrated for the various particle structures described above. Figure 9 presents the results of the relative viscosity of uniform suspensions and suspensions with loose and dense aggregates for various particle concentrations of the entire system. Although there is a large difference in the distribution of stresslets between uniform and aggregated suspensions as illustrated in Figs. 6 and 7, the viscosity shows only a little change. The inset of Fig. 9 shows a close-up of the viscosity in dilute

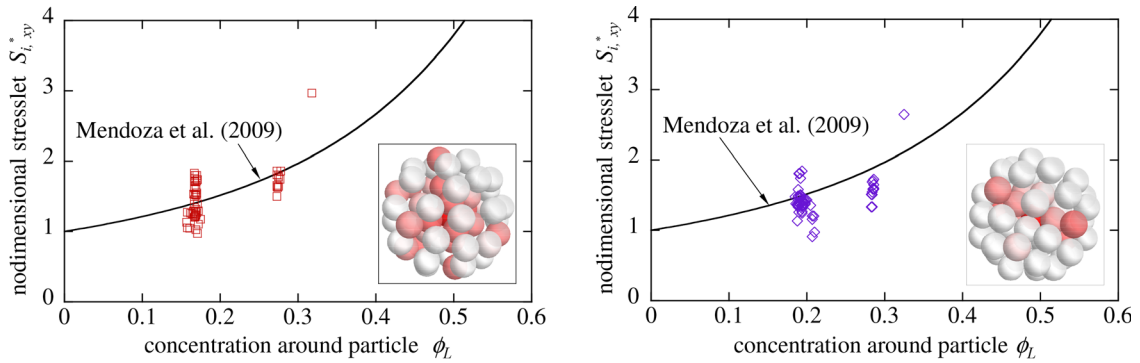


(a) $\phi = 0.01$ (b) $\phi = 0.15$

**FIG. 8.** Relationship between the stresslet and local concentration in aggregated suspensions: (a) $\phi = 0.01$ and (b) 0.15.

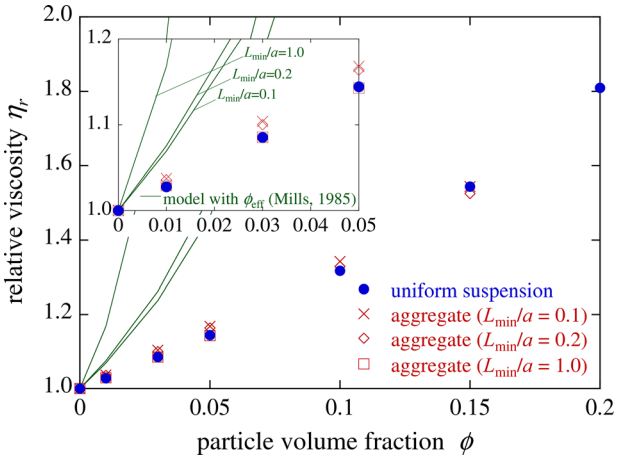


**FIG. 9.** Relationship between the relative viscosity and particle volume fraction for uniform and aggregated suspensions.

suspensions ($\phi = 0$–$0.05$). A detailed comparison of the results indicates that the viscosity of aggregated suspension is slightly larger than that of the uniform suspension; however, the difference is only several percent. The solid lines indicate the viscosity calculated from Eq. (48) with the effective volume fraction $\phi_{\text{eff}} = 4\pi R_{\text{agg}}^3/3V$, under the assumption that the interstitial fluid in the aggregate becomes entirely immobile for respective $L_{\min}/a$ conditions. The viscosity obtained from the analysis is much smaller than the results of Eq. (48), even in the case of dense aggregate ($L_{\min}/a = 0.1$). It can be said that the stresslet inside the aggregate changes due to hydrodynamic effects; however, the influence on the entire viscosity is not significant within the range of the calculation conditions, i.e., the aggregates composed of several tens of particles. At least, it is unlikely that the immobile fluid in the aggregate changes the viscosity by one to two orders of magnitude, even for larger aggregates. This result suggests that the direct contribution of inter-particle forces $\eta_r^I$, which is not considered here, is greater than the hydrodynamic contribution $\eta_r^H$ to the viscosity increase due to the formation of aggregates.

## CONCLUSION

A theoretical consideration of hydrodynamic effects on the rheological properties of particulate dispersions with aggregate structure was performed. The hydrodynamic transport coefficients, such as the permeability in the particle layer, the drag force in multi-particles, and the viscosity of suspension, were calculated theoretically by the multipole expansion of the particle velocity and the fluid force in reciprocal space. The results of the permeability and drag force were consistent with those obtained from previous studies over a wide range of particle concentrations. The viscosity of uniformly distributed particulate suspensions was also in good agreement with previous experimental results from small to large concentrations.

The hydrodynamic effects on the viscosity in aggregated suspensions were considered by examining the stresslet distribution in the aggregate. The stresslet in the aggregate shows larger values in the center as the particles become locally dense, and it almost corresponds to the theoretical stresslet calculated by local concentrations. It means that the stresslets of particles near the center of the aggregate are not influenced by other aggregates by the shielding effect.

The effective viscosity of particulate suspension did not change so much by aggregation in this analysis, i.e., the hydrodynamic effects play a minor role in determining the viscosity of aggregated suspension. This suggests that, at least in aggregates composed of dozens of particles, the direct contribution of inter-particle forces on the viscosity is significant in aggregated suspensions, which is contrary to the assumption of existing viscosity models.

## AUTHOR DECLARATIONS

### Conflict of Interest

The authors have no conflicts to disclose.

### Author Contributions

**Yutaro Tanii:** Investigation (lead); Writing – original draft (equal). **Namiko Kamata:** Investigation (equal); Methodology (equal). **Hiroki Saito:** Investigation (equal); Methodology (equal); Writing – original draft (equal). **Shusaku Harada:** Conceptualization (lead); Investigation (equal); Writing – original draft (equal). **Manabu Sawada:** Conceptualization (equal); Investigation (equal).

## DATA AVAILABILITY

The data that support the findings of this study are available from the corresponding author upon reasonable request.

## REFERENCES

[1]I. L. de Camargo, M. M. Morais, C. A. Fortulan, and M. C. Branciforti, "A review on the rheological behavior and formulations of ceramic suspensions for vat photopolymerization," Ceram. Int. **47**, 11906–11921 (2021).
[2]L. Pullum, D. V. Boger, and F. Sofra, "Hydraulic mineral waste transport and storage," Annu. Rev. Fluid Mech. **50**, 157–185 (2018).
[3]H. Chang, P. Zhang, R. Guo, Y. Cui, Y. Hou, Z. Sun, and W. Rao, "Recoverable liquid metal paste with reversible rheological characteristic for electronics printing," Appl. Mater. Interfaces **12**, 14125–14135 (2020).
[4]A. Einstein, "Berichtigung zu meiner Arbeit: Eine neue Bestimmung der moleküldimensionen," Ann. Phys. **339**, 591–592 (1911).
[5]W. B. Russel, D. A. Saville, and W. R. Schowalter, *Colloidal Dispersions* (Cambridge University Press, 1989).
[6]G. Bossis and J. F. Brady, "The rheology of Brownian suspensions," J. Chem. Phys. **91**, 1866–1874 (1989).
[7]J. N. Israelachvili, *Intermolecular and Surface Forces* (Elsevier, 1985).
[8]P. Mills, "Non-Newtonian behaviour of flocculated suspensions," J. Phys. Lett. **46**, 301–309 (1985).
[9]M. Kobayashi, Y. Adachi, and S. Ooi, "On the steady shear viscosity of coagulated suspensions," J. Soc. Rheol. Jpn. **28**, 143–144 (2000).
[10]A. Chougnet, T. Palermo, A. Audibert, and M. Moan, "Rheological behaviour of cement and silica suspensions: Particle aggregation modelling," Cem. Concr. Res. **38**, 1297–1301 (2008).
[11]A. J. C. Ladd, "Hydrodynamic interactions in a suspension of spherical particles," J. Chem. Phys. **88**, 5051–5063 (1988).
[12]A. J. C. Ladd, "Hydrodynamic interactions and the viscosity of suspensions of freely moving spheres," J. Chem. Phys. **90**, 1149–1157 (1989).
[13]A. J. C. Ladd, "Hydrodynamic transport coefficients of random dispersions of hard spheres," J. Chem. Phys. **93**, 3484–3494 (1990).
[14]P. Mazur and W. van Saarloos, "Many-sphere hydrodynamic interactions and mobilities in a suspension," Physica A **115**, 21–57 (1982).
[15]H. Hasimoto, "On the periodic fundamental solutions of the Stokes equations and their application to viscous flow past a cubic array of spheres," J. Fluid Mech. **5**, 317–328 (1959).

[16]K. Cahill, *Physical Mathematics* (Cambridge University Press, 2013).
[17]S. Kim and S. J. Karrila, *Microhydrodynamics* (Dover Publications, Inc., 2005).
[18]D. J. Jeffrey and Y. Onishi, "Calculation of the resistance and mobility functions for two unequal rigid spheres in low-Reynolds-number flow," J. Fluid Mech. **139**, 261–290 (1984).
[19]H. C. Brinkman, "On the permeability of media consisting of closely packed porous particles," Appl. Sci. Res. **1**, 81–86 (1949).
[20]P. C. Carman, "Fluid flow through granular beds," Trans. Inst. Chem. Eng. **15**, 150–166 (1937).
[21]M. A. van der Hoef, R. Beetstra, and J. A. M. Kuipers, "Lattice-Boltzmann simulations of low-Reynolds-number flow past mono- and bidisperse arrays of spheres: Results for the permeability and drag force," J. Fluid Mech. **528**, 233–254 (2005).
[22]D. L. Koch and A. S. Sangani, "Particle pressure and marginal stability limits for homogeneous monodisperse gas fluidized bed: Kinetic theory and numerical simulations," J. Fluid Mech. **400**, 229–263 (1999).
[23]R. J. Hill, D. L. Koch, and A. J. C. Ladd, "The first effects of fluid inertia on flows in ordered and random arrays of spheres," J. Fluid Mech. **448**, 213–241 (2001).
[24]G. K. Batchelor and J. T. Green, "The determination of the bulk stress in a suspension of spherical particles to order $c^2$," J. Fluid Mech. **56**, 401–427 (1972).
[25]G. F. Eveson, "The viscosity of stable suspensions of spheres at low rates of shear," in *Rheology of Disperse Systems*, edited by C. C. Mill (Pergamon Press, 1959), pp. 61–83.
[26]T. Shikata and D. S. Pearson, "Viscoelastic behavior of concentrated spherical suspensions," J. Rheol. **38**, 601–616 (1994).
[27]J. C. van der Werff, C. G. de Kruif, C. Blom, and J. Mellema, "Linear viscoelastic behavior of dense hard-sphere dispersions," Phys. Rev. A **39**, 795–807 (1989).
[28]H. C. Brinkman, "The viscosity of concentrated suspensions and solutions," J. Chem. Phys. **20**, 571 (1952).
[29]T. F. Ford, "Viscosity-concentration and fluidity-concentration relationships for suspensions of spherical particles in Newtonian liquids," J. Phys. Chem. **64**, 1168–1174 (1960).
[30]R. Simha, "A treatment of the viscosity of concentrated suspensions," J. Appl. Phys. **23**, 1020–1024 (1952).
[31]S. H. Maron and P. E. Pierce, "Application of Ree-Eyring generalized flow theory to suspensions of spherical particles," J. Colloid Sci. **11**, 80–95 (1956).
[32]S. H. Maron and A. W. Sisko, "Application of Ree-Eyring generalized flow theory to suspension of spherical particles. II. Flow in low shear region," J. Colloid Sci. **12**, 99–107 (1957).
[33]M. Mooney, "The viscosity of a concentrated suspension of spherical particles," J. Colloid Sci. **6**, 162–170 (1951).
[34]C. I. Mendoza and I. Santamaria-Holek, "The rheology of hard sphere suspensions at arbitrary volume fractions: An improved differential viscosity model," J. Chem. Phys. **130**, 044904 (2009).
[35]S. A. Adelman, "Hydrodynamic screening and viscous drag at finite concentration," J. Chem. Phys. **68**, 49–55 (1978).